

2D AND 3D INTAKES PERFORMANCE AND DRAG OF CRUISE M=1.6 CIVIL AIRCRAFT

Viacheslav A. Vinogradov, Vladimir A. Stepanov
Central Institute of Aviation Motors (CIAM), Russia,

Keywords: *2D and 3D intake, drag, throttle performance*

Abstract

Two high efficient intakes – 3D and traditional 2D consisted of supersonic inlet and subsonic large curvature diffuser were developed for supersonic business aircraft with $M_\infty=1.6$ cruise flight. Preliminary deceleration of incoming airflow and boundary layer control (BLC) in case of 3D inlet are provided by swept wedge placed in front of inlet due to the forming transverse pressure gradient. In case of 2D inlet bypass of BL is provided by installation of the inlet on bleed wedge of some height. Further compression is realized in a system of 3-D shocks with terminal normal one. Numerical modeling based on solution of 3-D Navier-Stokes equations allowed obtaining the results of inlet and subsonic diffuser flowing under the boundary layer suction in a throat at throttle modes under $M=0.8-1.8$. Results of calculation confirmed flow stability at 1.5..4-fold increased pressure in subsonic diffuser outlet section in comparison with external free stream pressure. It was received that using the BLC the total pressure recovery coefficient σ grows up to $\sigma = 0.89...0.97$ for considered M_∞ range. Drag evaluations of considered inlets with taking into account of additive and wave drag components and also wave drag of bleed wedge of 2D inlet resulted in approximately the same compression efficiency, but summary drag of 3D inlet is less by a factor of 1,5-3.5 times in comparison with 2D inlet drag at $M_\infty=0.8-1.8$ range.

1 Introduction

One of the advanced trends in the development of high speed flight vehicles powered by air breathing engines is the

tendency to use three dimensional (3-D) inlets. They submit wide variety of geometry schemes depending on inlet and engine requirements and necessity of compatibility with vehicle airframe. These schemes offer a potential increase in the compression efficiency as compared with 2-D traditional inlets. As the flows in 3-D inlets are rather complicated especially at off-designed modes of operation an efficient method for their designing and research is numerical designing and simulation of operation under required conditions based on RANS and LENS codes. The efficient way for designing 3-D schemes is so-called method of “gas dynamic” designing when surfaces of configurations follow the streamlines of required (known) flows. Among works on gas dynamic designing should be noted 1-3, where supersonic flow is compressed along the directions converging in space. Such convergent inlets first of all were considered applied to hypersonic flight vehicle inlets because of special requirements to their performance such as high efficient operation at wide Mach number range and small wetted surface of compression elements and duct. Small wetted surface of the duct contribute, in particular, further to reducing the inlet weight and facilitating the thermal protection of the propulsion at high flight velocities. Besides convergent inlets constructed with the use of flat and conical walls of swept leading edges are very attractive because of their constructive simplicity and flexibility of their integration together with the engine duct in the vehicle airframe.

The object of the present work is a continuation of research development 4, 5 of supersonic inlet for supersonic business aircraft (SBA) intended for cruise flight at $M_\infty=1.6$.

Among a number of SBA should be noted first of all now historical aircrafts “Concord” by French-England companies and “Tu-144” by Russian Design Bureau named after A. Tupolev, projects of Boeing in the USA, DASSAV in France and “Sukhoi” in Russia 6. These projects include different configurations of propulsions involving mainly axis-symmetrical and close to 2-D schemes arranged on the airframe fuselage or the wing. One of the common features of these propulsion projects is an aspiration to avoid capturing of thick boundary layer which is growing on aircraft nose part or wing surface, i.e. to organize control of boundary layer by bleeding, suction or spillage. These ways as a rule require moving aside on some height of inlet to bypass boundary layer, to bleed or to organize spillage or suction in the inlet throat region to enhance compression process and to provide stable operation of propulsion at wide flight and engine conditions.

In this work scheme of inlet and subsonic diffuser intended for SBA propulsion is analyzed. Two schemes of inlet are considered: inlet of traditional 2D scheme and 3D scheme close to 2-D configuration, but with the use 3-D constructive elements which make flow field in inlet and extra curvilinear subsonic diffuser as a complex three dimensional flow.

2 Statement of Work

The design methodology of inlet flow path and integration with flying vehicle (FV) airframe presented in work 2,3 is used for development of high efficient inlet with large curvature transient duct. The cardinal design principle is based on organization of flow deceleration in a system of weak spatial shocks and selection of compression surfaces coordinates in such a way so to avoid pressure gradients on duct walls bringing about boundary layer separation. The resulted inlet duct profile and outlet section flow parameters are used for designing curvilinear subsonic diffuser, integration with turbojet (GTE), and creation of high efficient propulsion inlet integrated with the supersonic business aircraft (SBA) airframe.

2.1 Purpose of study

The present work is aimed at:

- Design an uncontrollable auto-starting inlet intended for SBA cruising flight at $M_\infty = 1.6$, $q_\infty = 50 \text{ kPa}$ and zero angles of attack and slip and mounted on SBA fuselage or wing.
- Get local flow parameters and integral performance of inlet and subsonic diffuser (SD) compression process.
- Develop the system of bleeding and control of boundary layer forming on SBA surface for prevention of flow separation and ensuring stable inlet operation at throttle modes and GTE matching.
- Calculation and comparison the values of shock and additive drags of considered inlets under condition of equal captured airflow rates and stable inlets operation under SD flow throttling.

2.2 Requirements and conditions of designing

Design and choice of SBA 3D inlet configuration have been fulfilled under the following requirements:

- flight at wide range of $M_\infty \leq 1.8$ and $q_\infty = 50 \text{ kPa}$ (variable flight altitude) with cruising flight at $M_\infty = 1.6$;
- typical frontal inlet area size – $A_{\text{inlet}} = B \times H = 1 \times 1 \text{ m}^2$;
- inlet is arranged on FV fuselage or wing and located at a distance of 10m from leading edge;
- zero angles of attack and sideslip of inlet;
- SD diversion from inlet throat section up to engine inlet section makes up 1.12, ratio of inlet frontal area to subsonic diffuser exit is 0.88.

2.3 Design features of 3-D inlet

A 3-D self-start mixed compression inlet is considered for SBA propulsion, Fig. 2 and Fig. 3, which is characterized by the following features of geometric scheme and compression process organization:

1. Inlet geometry sizes are fixed and there are no moving control parts at considered flight regime.

2. Flow deceleration is provided by a system of oblique spatial shocks and terminal normal shock before the curvilinear “aggressive” subsonic diffuser or inlet entrance depending on throttling mode.
3. Initial deceleration of incoming flow is realized on the bleeding wedge with a flow turn angle of $\approx 7^\circ$ in a plane parallel to inlet axis. Leading edge of bleeding wedge is swept with an angle 45° on direction to free stream velocity vector.
4. Inlet cowl in plan is chosen with swept leading edge and angle of 45° for matching the shocks at flowing over the swept bleeding wedge. An initial inner cowl angle is zero relative to undisturbed flow $M_\infty=1.6$ and further inner compression is realized in two oblique shocks with flow turn angle of 7° each shock and terminal normal shock depending on throttle ratio $= p_{thrott} / p_\infty$, where p_{thrott} is a pressure at subsonic diffuser outlet section.
5. Inlet auto start at all the flight modes and stable flow at its throttling are ensured by the absence of lateral flaps on length from the cowl leading edge up to the bending section of bleeding wedge surface.
6. There is a preliminary bleed of the boundary layer (BL) at a section of external compression up to inlet duct section for flow control and decreasing negative influence of BL, Fig. 3. Under the pressure gradient resulted in flowing the swept wedge the most part of incoming boundary layer is removed to side direction before entering the inlet. The rest small BL part is captured by the inlet. This method of BLC was earlier offered for hypersonic inlets [7] and experimentally studied. Under its use a hypersonic inlet started up under smaller throat area since throat boundary layer separation area was diminishing.
7. Further boundary layer control in the considered inlet is realized by means of its suction through a slot length of $L_{slot}/D_{exit} = 0.089$ in the throat area due to pressure drop in the throat area and ambient flow. The bleed slot is run on rectilinear duct section on its whole width.
8. Behind the bleed slot a rectangular in initial section the subsonic diffuser duct smoothly goes first in hexahedron and then in a circle by diameter $D_{exit} = 1.0576\text{m}$. Subsonic diffuser duct area on length $LSD/D_{exit} = 2.84$ increases 1.12-fold close to linear change on length and subsonic diffuser axial line vertical displacement on condition of integration with airframe makes up $\approx 0.71 \times D_{exit}$, Fig.2. SD duct contour geometry for its entering in calculations is smoothed by spline of the third order. The subsonic diffuser outlet is docked with a constant area section by length $\approx 0.32\text{m}$.

2.4 2D inlet prototype

2D inlet of traditional scheme was chosen as a prototype for comparison of performance and drag components. Main features and dimensions are illustrated in Fig.4. At cruise designed Mach number $M=1.6$ deceleration of free stream flow is provided by four inclined shock waves of flow turn equal to $4, 5.1$ & 4.9° along the compression surface and 5° rejected shock on cowl and last terminal normal shock just before inlet entrance. 2D inlet is installed on bleeding wedge of 25° semi angle and H_{bl} , wedge $= 0.2H$ to exclude capturing of boundary layer growing on fuselage or wing. Inlet entrance dimensions are accepted the same as for the 3D inlet. Throat suction of boundary layer is performed through the slot of 0.03m length spreading along the whole duct width on distance of 0.158m downstream point K, Fig.4. Subsonic diffuser behind the throat section was designed the same as in case of 3D inlet with the exception of full inlet length equal to $L_{inlet+SD} = 5.12\text{m}$. SD diameter and exit area were equal to 1.1m and 0.944m^2 correspondingly.

2.6 Design features of 2-D inlet

Design conditions 1-3 for 2D inlet are the same as in a case of 3D inlet. Other items are the following:

4. Leading edge of cowl is perpendicular to X inlet axis and inner cowl angle was increased up to 9° to decrease total pressure

losses at cruise regime. Last choice will cause increase of nacelle drag.

5. Supersonic part of compression surface was fenced by side walls to increase inlet capture ratio.
6. There is preliminary bleeding of boundary layer growing along the compression surface and on the one hand it will increase captured flow rate, but on the other hand the region of inlet stable operation under throttling will decrease.
7. Throat suction of boundary layer is provided through the slot of 0.03m length.
8. Subsonic diffuser is similar with the 3D intake diffuser but with $L_{SD}/D_{exit}=3.48$ and increased exit area by a factor of 1.18.

3 Methodology of calculation

Calculation is conducted by means of integrating of Reynolds-averaged Navier-Stokes equations describing 3-D viscous compressible gas flow in the Cartesian coordinates system. A numerical method is used to solve the problem, which allows calculating spatial viscous flow of ideal gas with constant heat capacity in process of determination on time 3-5. In the numerical 2nd order approximation scheme, the procedure of rupture decomposition is used for calculation of flow parameters on lateral cell edges, which allows getting convergence in the presence of strong gradients of flow parameters. To describe turbulent features in different flow areas the two-parameter « κ - ε » turbulence model is used offered in works 9, 10.

Different fields of flow are studied under various boundary conditions. Adhesion conditions are set forth for viscous flow on walls ($q_w = 0$, where q_w – velocity vector on the wall). The wall parameters are defined from the "wall laws" for turbulent flow. On the left-hand border (entry in duct) assigned are pressure, temperature, absolute velocity vector (its module and direction), values of turbulence energy κ and dissipation velocity ε . Besides, at duct inlet and outlet are set zero derivatives of flow parameters. On the lateral borders of design area is assigned the "distortions non-reflection" condition, which assumes setting the "left" Ryman's boundary invariant. As initial

conditions ($\tau=0$) for all regions of the flow fields are set free flow parameters. At inlet outlet is set a combined boundary condition as the value of static pressure, which variations are modeling different inlet outlet's modes possible to appear under joint operation with the engine. If in outlet section there are reverse flows in the process of setting solutions, then in this case the values of velocity and temperature are defined from the condition of constant total enthalpy equal to the free stream flow. Calculation has shown that in the solutions obtained the outlet section velocity is always positive. The problem is settled by using regular net of rectangular cells of total amount up to $\approx 2 \times 10^6$ cells adapted for calculation of viscous near wall layers, best boundary layer resolution, and adequate flow core solidity. The whole region of calculation is divided in sub-areas in accordance with the peculiarities of flow and inlet geometry.

The system of Reynolds-averaged Navier-Stokes equations is solved in the process of time-sharing flow parameters in all areas under preset boundary and initial conditions. Integration on time is run by the implicit scheme and on each time-pitch a solution is found out by means of the determination method on flow parameters. The time-pitch is defined from the condition of stable convergence and depends on flow features.

4 Results of calculation and discussion

The SBA inlet is designed assuming air flow at $M_\infty = 0.8-1.8$ and variable flight altitude ($q_\infty = \text{const} = 50$ kPa) and zero angles of attack and sideslip, boundary layer forming on a plate of length 10m imitating airframe nose or wing surface for typical SBA configurations, Fig. 1. The mathematical image of 3-D inlet is shown in Fig. 5. Calculation of inlet and SD flow field for selected geometric sizes is executed for a half real inlet due to its configuration symmetry. Obtained are distributions of local flow parameters p , M , V , etc. on inlet length and its total performance inlet total pressure recovery σ and capture ratio φ coefficients, Mach number M_{aver} etc. in intermediate and outlet inlet

sections. Total features are defined by averaging of local parameter values on area.

4.1 Incoming boundary layer control

Normalized values of boundary layer thicknesses formed along an imitated plate of 10 and 20m length referred to inlet 1m height at $M_\infty=1.6$ are 0.15-0.25. Therefore decelerating in 3-D inlet is so organized to delete larger part of boundary layer before its entry in the inlet duct combining boundary layer bleeding and suction processes. Normally, the 2-D inlet is placed on the bleed wedge to bypass most boundary layer aside avoiding the inlet entrance, Fig.4. In case of 3D inlet swept wedge is used to decelerate flow and to organize bypass of boundary layer. Besides, in the throat region it is also necessary to use boundary layer bleeding or suction for prevention of flow stall when inlet operates on regime of deep throttling.

The BLC system of considered 3-D inlet includes a preliminary reduction of the boundary layer thickness on fore body formed by means of swept bleed wedge, Fig.2 and 3, and suction of boundary layer through the slot placed in throat area on lower inlet surface, Fig.3. Preliminary BLC effect is explained by pressure gradient appearing on bleed wedge under the flowing it which acts on flow streamlines. For illustration the pictures of streamlines chosen at different distances from the wall and corresponding to local inlet Mach number values are presented in Fig.6 & 7 for the considered inlets at $M_\infty = 1.6$. Under the flowing of swept wedge a flow is turned both in vertical and lateral directions. Resulted in pressure gradient acts on streamlines and causes flow deflection to lateral sides. Flow deflection is that more, than its velocity less, i.e. a streamline is closer to wall. Note that for the most part of swept wedge length ($X>0.7m$) at periphery ($Z/B_{inlet}=0.5$) pressure is less 8-10% opposite at $Z=0$. In case of weak throttling the streamlines on bleed wedge do not change their trajectories. With an increase of throttling high pressure comes upstream and reaches suction zone, causing an intensification of suction process and the rate of air through the slot and outside. Further increase of throttling results in

a formation of 3-D flow separation zone before the inlet entrance and some streamlines pass by inlet duct and so the captured airflow is decreased. Last phenomena causes decrease of pressure in the throat area and results in the decrease of suction flow. Continuation of throttling intensity again results in bypass flow rate, but the flow field is remained stable without any flow stall. Formation of separation zone before the inlet entrance nevertheless does not cause any stall in inlet and bypass of air is realized at small angles with regard to a direction of the main flow. When initial thickness of boundary is increased, Ref.5, bleeding is intensified up to large distance from the wall. So a drag of such airflow bypass is less in comparison with a drag of bypass in case of 2-D inlet when a normal shock is formed before the cowl as a rule. But at distance $Y/H_{inlet} = 0.5$ the streamlines in 3D inlet practically does not deflect from direction corresponding to non separated flow along bleed wedge at $M_\infty=1.6$, i.e. does not interact with bypass zone near crossing of bleed wedge and inlet side wall.

In case of 2D inlet a bypass of some airflow through the non-attached shock wave before the cowl leading edge at $Y/H=0.95$ caused by the strong throttling is realized and streamlines turn up, Fig.7. It results in increase of additional drag and decrease of propulsion efficiency.

4.2 Flow field features in inlet and subsonic diffuser duct

Examples of flow pictures in considered inlets – isolines of Mach number M and normalized static pressure p/p_∞ in XoY plane of the duct symmetry are shown in Fig.8 & 9 for the modes with variable throttle ratio of $\overline{p_{thrott}}$ at $M_\infty = 1.2$ and 1.6 and fuselage length of $L_f=10m$. Distributions of Mach numbers and total pressure recovery coefficient σ in outlet cross section of SD are shown in Fig.10 & 11 for the same regimes. Values of inlet capture ratios ϕ based on area averaged airflow rates through the inlet duct at different cross sections (Fig. 3) are given in Fig. 12.

Presented results show that pressure increase at subsonic diffuser exit, that is throttling of inlet makes a maximal effect on flow field in inlet duct and level of bleeding before the entrance of inlet and suction in the its throat, Fig.13.

When level of throttling is increased a pressure spreads upstream along the subsonic part of boundary layer and reaches suction zone in the throat. As pressure drop between this zone and outside pressure is increased then flow rate through the slot is increased also, Fig.12. At some value of $\overline{p_{thrott}}$ the region of disturbed flow appears before the inlet entrance and some air streams deflect from previous direction and do not enter inlet. Flow field in diffuser is subsonic and flow rate through the suction slot grows. Under large levels of $\overline{p_{thrott}}$ (but not maximal ones) growing of suction air flow is decreased and continuation of throttling intensification results in increase of air bleeding before the inlet entrance and decreasing of captured air flow rate by the inlet.

Analogous behavior of flow field under the throttling is realized in 2D inlet. When M_∞ is decreased and acts strong throttling a normal shock wave appears before the cowl leading edge and supersonic flow is broken. Such airflow bypass just before the cowl is realized at rather large angles. In case of 3D inlet flow bypass is realized under the lower angles with respect to the free stream flow direction and so the drag of bleeding for such inlet configuration will be less than the bleeding with the presence of the normal shock which is typical for the 2-D inlet.

Analysis of results in Figures 6-17 presented permits to conclude:

1. Flow field in 3D inlet and subsonic diffuser under all studied operation modes at $M_\infty = \text{var}$ and $L_f = 10\text{m}$ with throttling is stable in spite of 15-25% decrease of flow rate before the inlet entrance (on bleed wedge and in suction zone) and pressure increase in exit SD cross section $\overline{p_{thrott}}$ up to 1.5-5 times. When throttling is increased a terminal shock wave goes upstream, Fig.8 & 9, and it is stabilized in the region of cowl leading edge at maximal value of

$\overline{p_{thrott}}$, Fig. 8 & 9. It should be noted that even under maximal throttling of similar inlet at $M_\infty = 1.6$ (Ref. 4) followed by flow rate decrease by 30-40% in comparison with initial operation regime the flow field in inlet was stable without separation zones near cowl and side walls.

2. Under the throttling the inlet capture ratios φ are decreased depending on M_∞ and value of throttling, Fig.13-14.

3. At $M_\infty = 1.6$ the suction flow rate at throat region is growing up to 4-5% of total flow rate. At large throttling a stability of flow in inlet duct is ensured mainly by the flow bypass of incoming flow at external compression region on bleed wedge before the inlet entry. In cases of inlet operation without throttling at $M_\infty = 1.2$ and 1.4 some injection (0.3-0.5%) of air into the throat area from the suction system was observed.

4. There are no zones of reverse flow at SD exit section in spite of small length of SD and its large curvature S-shaped configuration. With increase of $\overline{p_{thrott}}$ the distributions of flow parameters becomes more uniform, Fig.10, 11 & 17 and total level of σ values in inlets becomes larger by 5-10% in comparison with operation without throttling for both inlets.

5. Region of stable operation $\Delta\overline{\varphi_{thrott}} = (\varphi_{\max} - \varphi_{\min})/\varphi_{\max}$ of 3D inlet under the throttling is larger than 2D inlet region and so 3D inlet is more acceptable for concordance with the propulsion control system.

4.3 Summary and throttle performance of inlets

Basing on calculation results of local flow field parameters the total pressure σ and capture ratio φ coefficients and Mach number M_6 (exit area averaged data) and throttle performance $\sigma = f(\varphi)$ of 3-D and 2D inlets combined with short subsonic diffuser under $M_\infty = 0.8-1.8$ flowing were defined and given in Fig. 13. Here percentage values of suction flow rate in the throat region are presented depending on total inlet flow rate.

Extreme left points of 2D throttle performance, Fig.13b, characterize almost maximum $\overline{p_{thrott}}$ values and an increase by 2-5% over these ones led to flow disruption and as a consequence caused strong decrease of capture ratio and inlet efficiency. But thanks to BLC by swept bleed wedge in 3D inlet a bypass of flow rate at throttling regimes is provided mainly in shock system of rather weak intensity. So in case of 3D inlet an increase of SD exit pressure by 10-30% over extreme left points in throttle performance, Fig.13a, we had smooth decrease of inlet capture ratio under approximately constant total pressure losses. At least disruption of flow field was not realized in calculative research.

Summary σ & φ values corresponding to its maximum values (so-called “angle” points on $\sigma=f(\varphi)$ dependence) in Fig.13 data and to possible regimes of stable joint inlet/engine operation are given in Fig.14. One can see when level of throttling is increased and as a result averaged Mach number is decreased, Fig.15 the losses of total pressure in inlet/subsonic diffuser system are decreased, Fig.16. Confirmation of conclusion about decreasing of flow non uniformity at exit section in Fig.10, 11 is data in Fig.17, where parameter $\Delta\sigma$ of flow non uniformity was presented versus exit averaged Mach number M_6 . Value of $\Delta\sigma$ was evaluated according with equation $\Delta\sigma = \Sigma\{abs(\sigma_i - \tilde{\sigma}) \times A_i\} / (A \times \tilde{\sigma})$, where σ_i and $\tilde{\sigma}$ - local and area averaged meanings of total pressure recovery coefficient and A_i and A – are values of local and summary exit diffuser area. As it was proposed when Mach number M_∞ is grown and level of throttling is decreased the $\Delta\sigma$ values are increased. At $M_\infty=1.8 > M_{dsgn}$ non uniformity of 3D inlet becomes in a factor by two larger in comparison with operation at $M_\infty \leq 1.6$, Fig.17b. In case of traditional 2D inlet the level of non uniformity are on the same level, Fig.17a.

Scheme of 3D inlet (only half of inlet because of its symmetry) with explanation of calculative methodology and referred surfaces is given in Fig.18. Drag of inlet nacelle was calculated directly by summarizing of forces acting on nacelle planes by line drawn marked.

In case of additive drag the force F_{add} acting on “liquid” contour, Fig.18, was calculated from equation of impulse written in projection to X axis for the flow stream between cross sections « ∞ » & «entry». For convenience, F_{add} was summarized with drag force acting on some bleed wedge surface which is flowing by air not entered inlet.

$$F_{add,eff} = F_{add} + F_{wedge} \times (1 - k) = I_{entr} + F_{wedge} \times k - I_\infty \times \varphi + F_{wedge} \times (1 - k) = I_{entr} + F_{wedge} - I_\infty \times \varphi$$

Here I is a total impulse of air flow in cross sections « ∞ » & «entry», $F_{wedge} = \int (P_w - P_\infty) dA_{wedge}$ – force acting on swept bleed wedge, F_{add} – force acting on limit streamline surface and equal to $F_{add} = \int (P_i - P_\infty) dA_{add}$. Coefficient k is equal to the part of total wedge surface flowing by air entering inlet. Value of k was defined from consideration pictures of streamlines on inlet bleed wedge, Fig. 6 & 7 and Ref. 4, 5. Value of drag force was normalized by referring to dynamic pressure of free stream flow $(\rho \times U^2)_\infty$ and inlet entrance area A_{entr} equal to $1m^2$.

Calculation of 2D inlet drag was performed with the use the same methodology, but with account for drag force $F_{bl\ wedge}$ of bleed wedge on which the inlet was installed, Fig.4. Besides the drag of side walls compression surface bounded was added to drag of nacelle.

Values of additive drag and nacelle drag coefficients for considered inlets are given in Fig.19 & 20. Drag of bleed wedge applied by 2D inlet is presented in Fig.21. Summary values of drag $C_{X_{inlet}} = C_{X_{add}} + C_{X_{nacelle}} + C_{X_{bl.w}}$ for considered 2D and 3D inlets are presented in Fig.22. Here the same data are given for 2D inlet with straight subsonic diffuser. As it was proposed drag components of 3D inlet less than 2D inlet ones both at cruise regime and regimes of acceleration at $M_\infty = 0.8-1.4$, and these benefits will be able to compensate slightly worse performance σ and φ of 3D inlet in comparison with data of 2D inlet. However, final requirements to inlet performance and “price” of each parameter should be elaborated under complex evaluation of SBA performance and, for example, range of SBA with different propulsion.

5 Conclusions

Designed and developed the configurations of traditional 2D and new scheme 3D auto starting non controllable inlets combined with S-shaped subsonic diffuser for supersonic cruise $M_\infty=1.6$ business aircraft propulsion on fuselage or wing arranged.

Numerical research of flow field in inlet duct and subsonic diffuser was conducted and compression performance efficiency φ , σ , $\Delta\sigma$, M_{exit} were evaluated at Mach number $M_\infty=0.8-1.8$ range at zero angles of attack and sideslip and boundary layer thickness corresponding to fuselage length of 10m with and without throttling effect.

It was shown that flow field in 3D inlet is stable without stall under the pressure increase at subsonic diffuser exit up to $\frac{p_{thrott}}{p_\infty}=1-4.5$ при $M_\infty=0.8-1.8$ thanks to boundary layer bleeding (bypass) before the inlet entrance (8-15%) and suction in the inlet throat region (2-5%). φ and σ performance of traditional 2D inlet are slightly higher than ones for the 3D inlet, but 3D inlet is more attractable because of lower wave and additive inlet drags.

The inlets performance at exit subsonic diffuser on proposed joint inlet/engine operation regimes are equal to $\sigma = 0.95 - 0.88$ and $\varphi=0.72-0.84$ correspondingly under the flight Mach numbers increase from 0.8 up to 1.6. Losses of total pressure in subsonic diffuser do not exceed 1% and total pressure non uniformity parameter $\Delta\sigma$ does not exceed 4-6% at $M_\infty \leq 1.6$ at the same regimes of operation.

It was confirmed that total drag of 2D inlet is higher than for 3D inlet by 1.5-3.5 times under increasing flight Mach number in a range of 0.8-1.8.

References

[1] Goonko, Yu.P., Zatuloka, V.V., and Yuditsev, Yu.N., "A Class of Hypersonic Aircraft Configurations with Convergent Inlets Designed by Combining V-shaped Bodies", In a book (collected papers) "Hypersonic Aerodynamics Research" published by Institute of Theoretical and Applied

- Mechanics, Novosibirsk, Russia, 1978, pp. 68-84, (in Russian).
- [2] Smart, M., "Design of 3-D Hypersonic Inlets with Rectangular-to-Elliptical Shape Transition", Journal of Propulsion and Power, Vol. 15, No. 3, pp.408-416, 1999.
- [3] Borovikov, A., Gavrilouk, A., Gilevich, I., Duganov, V., Khokhlov, A., Stepanov, V., "Gasdynamic design of supersonic and hypersonic airframe integrated inlets and nozzles", AIAA Paper 96-4549, 1996.
- [4] Vinogradov, V., Stepanov, V. "Scheme and Inlet Performance of Supersonic Business Aircraft", AIAA Paper 2008 - , presented at 44th Joint Propulsion Conference, Hartford, 20-23 July 2008.
- [5] Vinogradov, V.A., Stepanov, V.A. "Scheme and Inlet Performance of Business M=1.6 Cruise Aircraft", AIAA Paper 2009-035, 47th Aerospace Sciences Conference, 2009, Orlando, 5-8 Jan. 2009.
- [6] Wall, R., "Gaining Speed", Aviation Week & Space Technology, No.12, March, p.43, 2007.
- [7] Vinogradov, V., Ogorodnikov, D., "Numerical and Experimental Study of Performance and Starting of 2-D Hypersonic Inlets", Technical Bulletin of CIAM, No.1, 1971, (in Russian).
- [8] Vasil'ev, V., Zakotenko, S.N., Krashenninnikov, S.Yu., Stepanov, V.A., "Numerical Investigation of Mixing Augmentation Behind Oblique Shock Waves." AIAA Journal, Vol. 32, No.2, 1994.
- [9] Gulyaev, A.N., Kozlov, V.E., Secundov, A.N., "Creation of one-parametric Model of Turbulent Viscosity", Izvestiay of Russian Academy of Sciences, Mekhanika i zidkosti I gaza, No. 2, 1993.
- [10] Kozlov, V.E., Secundov, A.N., Smirnova, I.P., «Turbulence Models for Flow Prediction in Gaseous Compressible Jet», Izvestiay of Russian Academy of Sciences, Mekhanika i zidkosti I gaza, No. 6, 19864 Copyright Issues

Copyright Statement

The authors confirm that they, and/or their company or organization, hold copyright on all of the original material included in this paper. The authors also confirm that they have obtained permission, from the copyright holder of any third party material included in this paper, to publish it as part of their paper. The authors confirm that they give permission, or have obtained permission from the copyright holder of this paper, for the publication and distribution of this paper as part of the ICAS2010 proceedings or as individual off-prints from the proceedings.

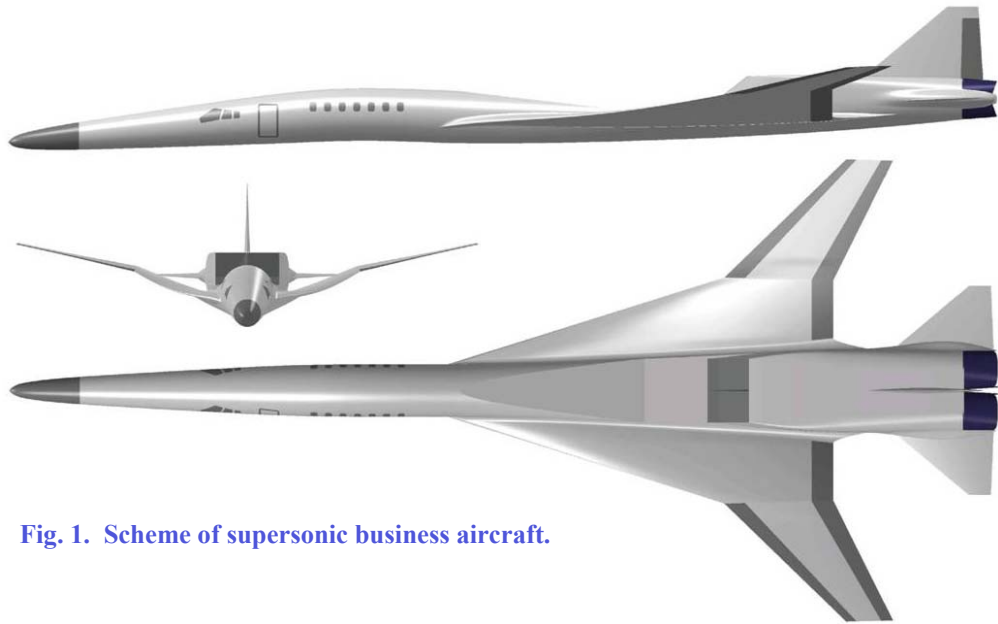


Fig. 1. Scheme of supersonic business aircraft.

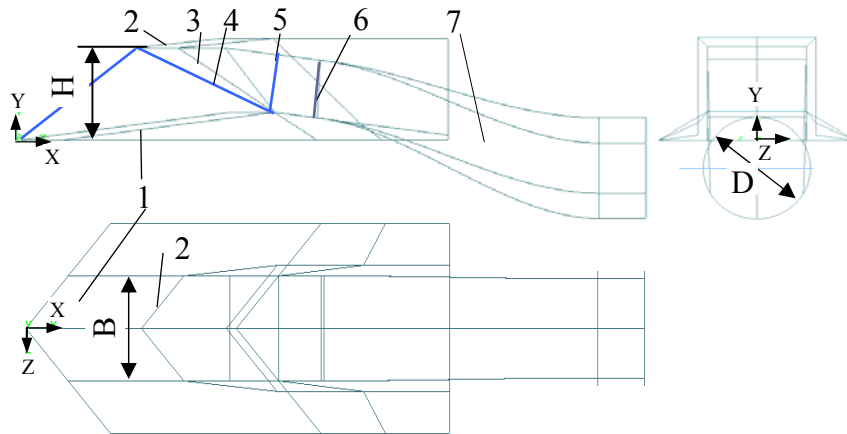


Fig. 2. Schematics of 3-D inlet

1 – bleed wedge and pre-compression surface, 2 – leading edge of cowl, 3 – leading edge of side wall, 4 – oblique shock wave, 5 – terminal shock wave, 6 - subsonic diffuser entrance, 7 – curvilinear diffuser

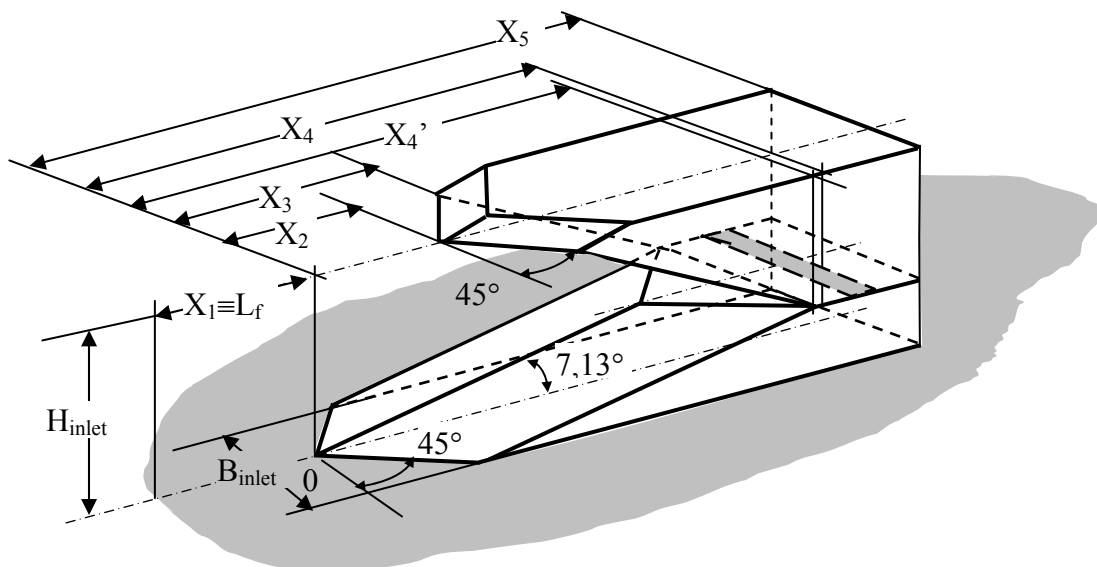


Fig. 3. Schematics of 3-D inlet for SBA (subsonic diffuser was not shown): $X_1=10m$, $X_2=1m$, $X_3=1,5m$, $X_4=2.387m$, $X_6=5.766m$, $X_4'=2.1m$, X_6 value corresponds to inlet with subsonic diffuser

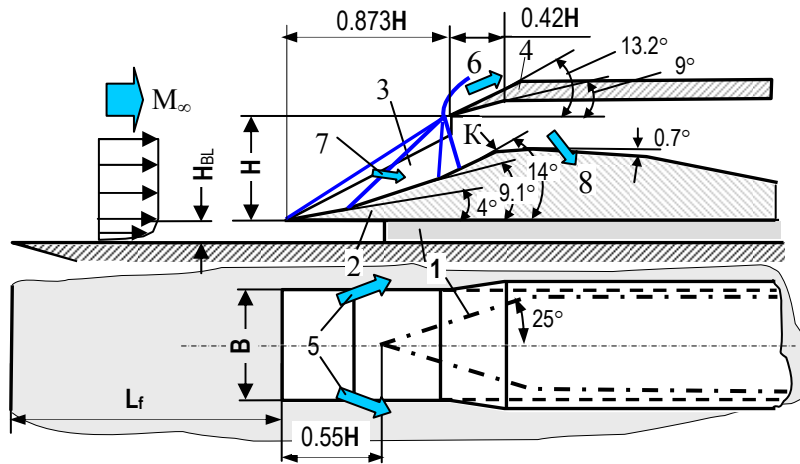


Fig. 4 . Scheme and main dimensions of 2D inlet (without subsonic diffuser):
 1 – bleeding wedge, 2 – compression surface, 3 – side surface, 4 – cowl, 5 – air bypass before bleeding wedge, 6 – air bleeding before cowl, 7 – air bleeding out of side walls, 8 – throat suction through slot

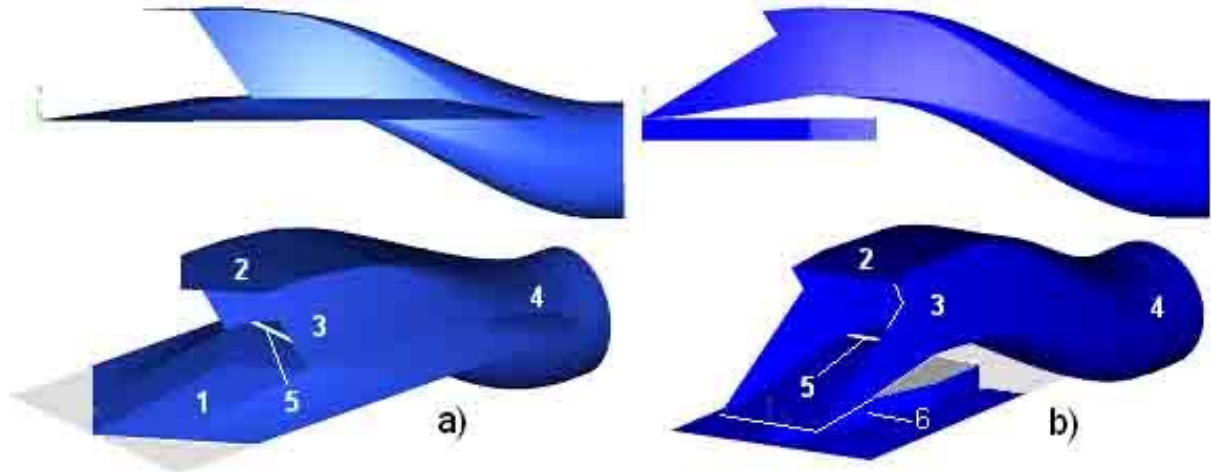


Fig. 5. Computational domains of inlets: a - 3D & b - 2D inlet
 1 – precompression wedge for bleeding of boundary layer, 2 – cowl, 3 – side wall, 4 – curvilinear subsonic diffuser, 5 – suction slot, 6 – bleed wedge

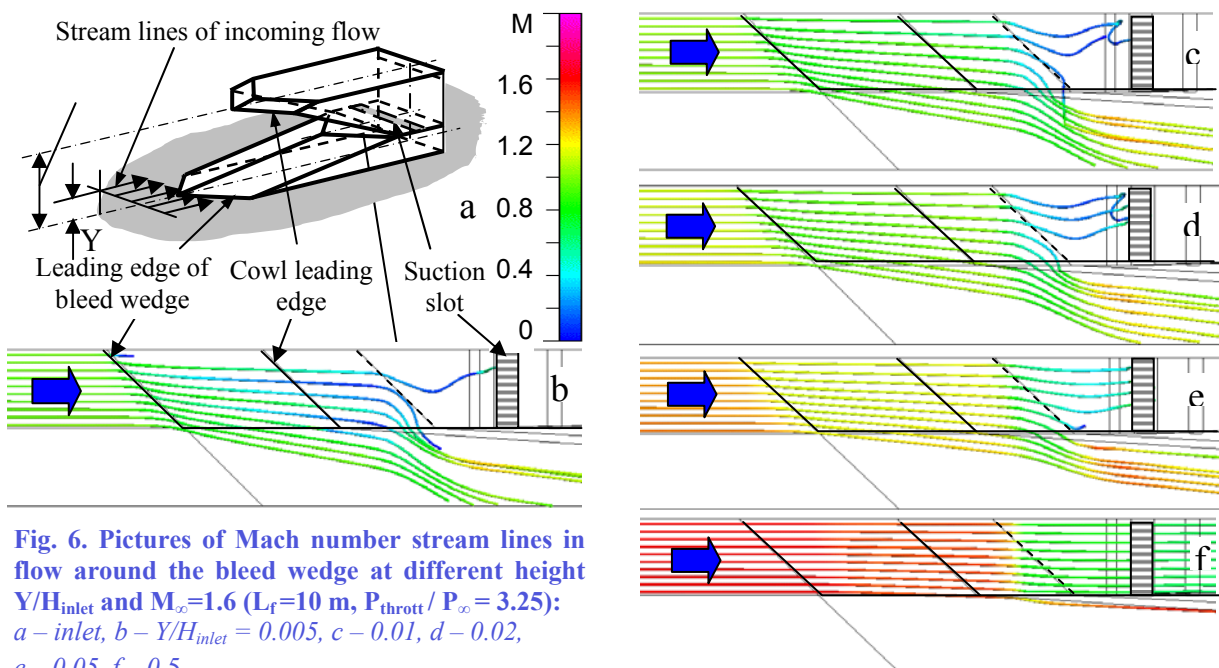
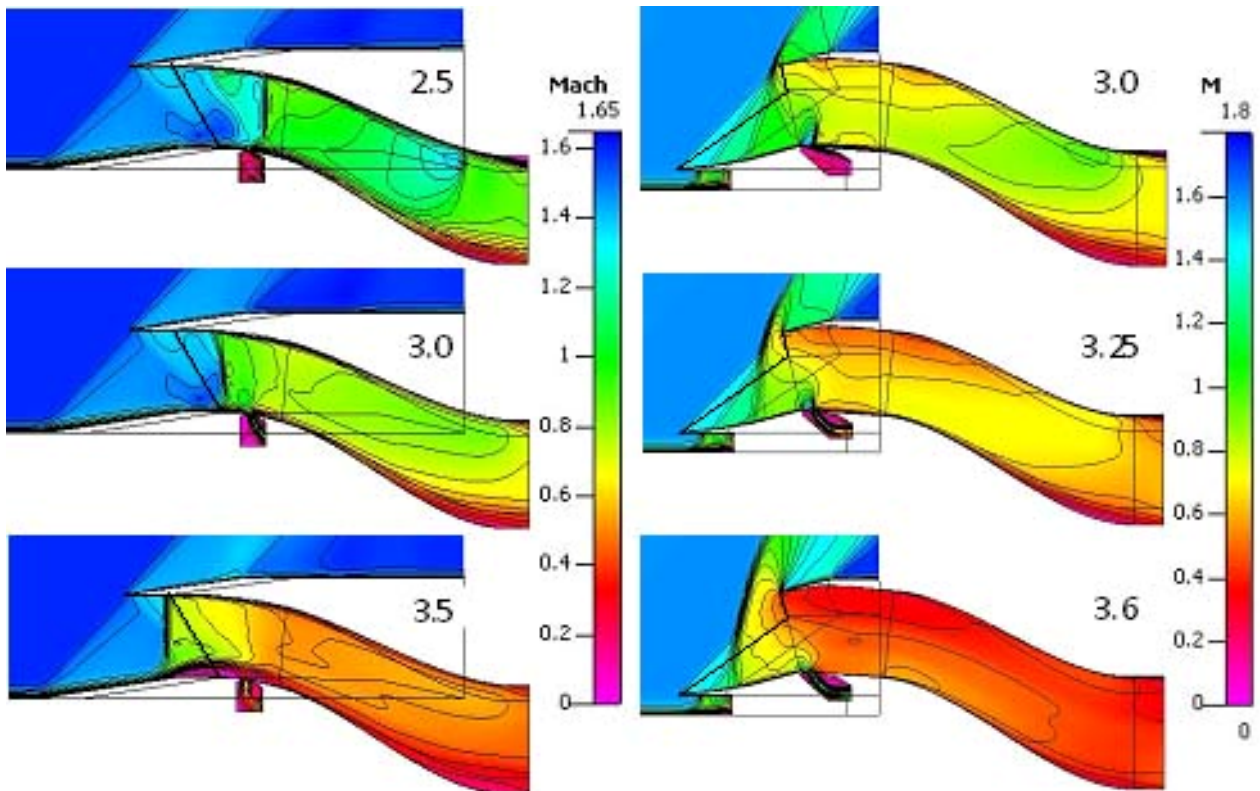
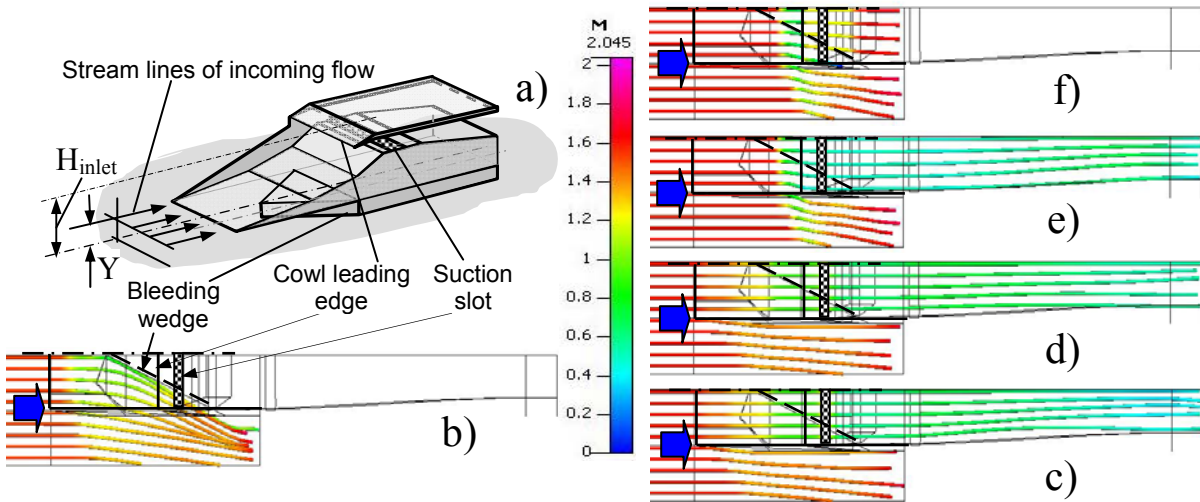


Fig. 6. Pictures of Mach number stream lines in flow around the bleed wedge at different height Y/H_{inlet} and $M_\infty=1.6$ ($L_f=10$ m, $P_{thrott} / P_\infty = 3.25$):
 a – inlet, b – $Y/H_{inlet} = 0.005$, c – 0.01, d – 0.02, e – 0.05, f – 0.5



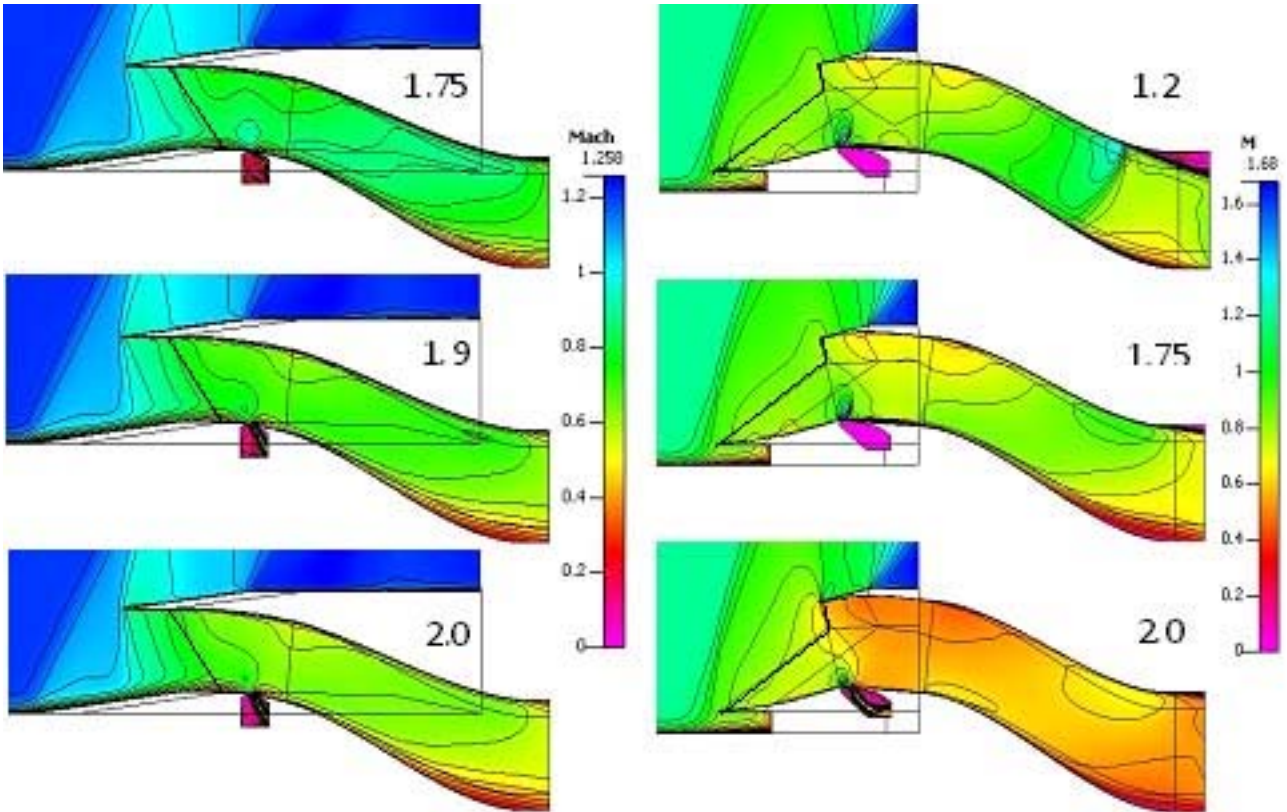


Fig. 9. Flowfield pictures ($M=\text{const}$ isolines) for 3D (left) and 2-D (right) inlets symmetry plane at $M_\infty=1.2$ and $L_f=10m$ with suction under different level of throttling (figures in pictures correspond to level of throttling P_{thrott} / P_∞)

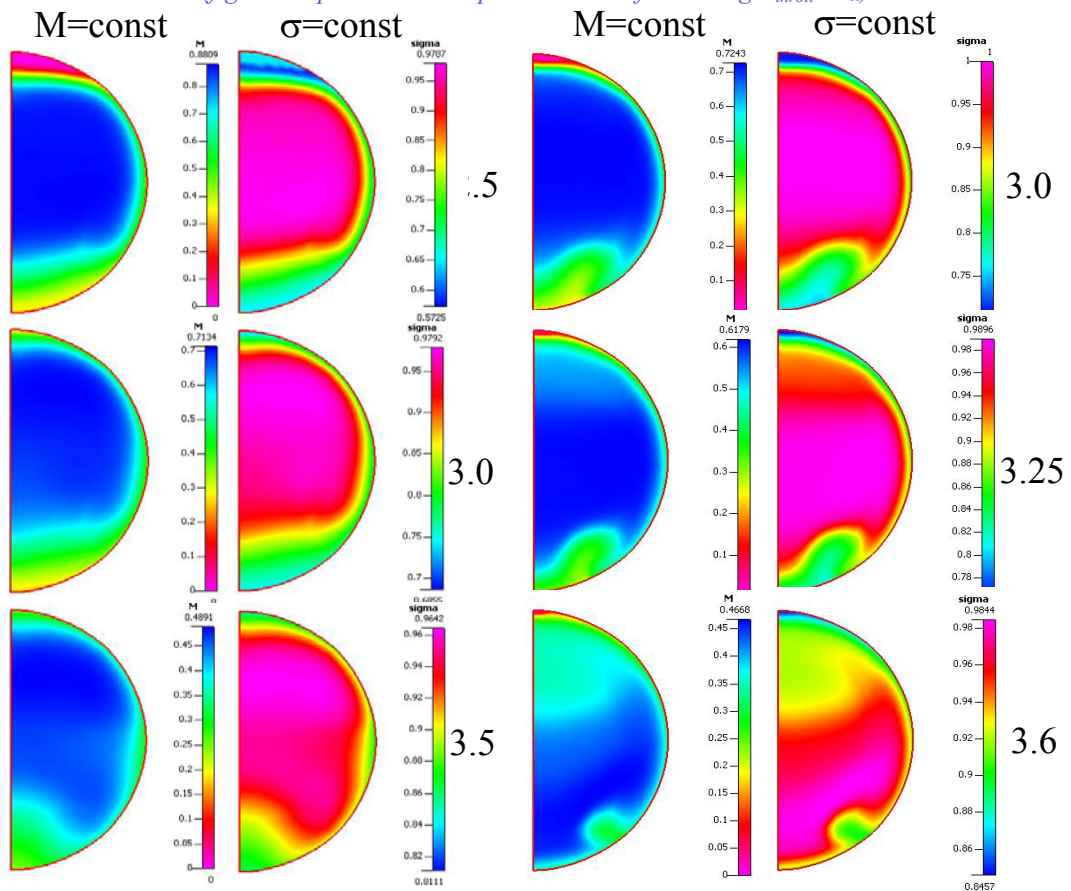


Fig. 10. Flow parameters - Mach number M and total pressure recovery coefficient σ at subsonic diffuser exit of 3D (left) and 2D (right) inlets under $M_\infty=1.6$ and throttling regime operation (figures in pictures correspond to $P_{thrott} / P_\infty = \text{var}$).

2D AND 3D INTAKES PERFORMANCE AND DRAG OF CRUISE M=1.6 CIVIL AIRCRAFT

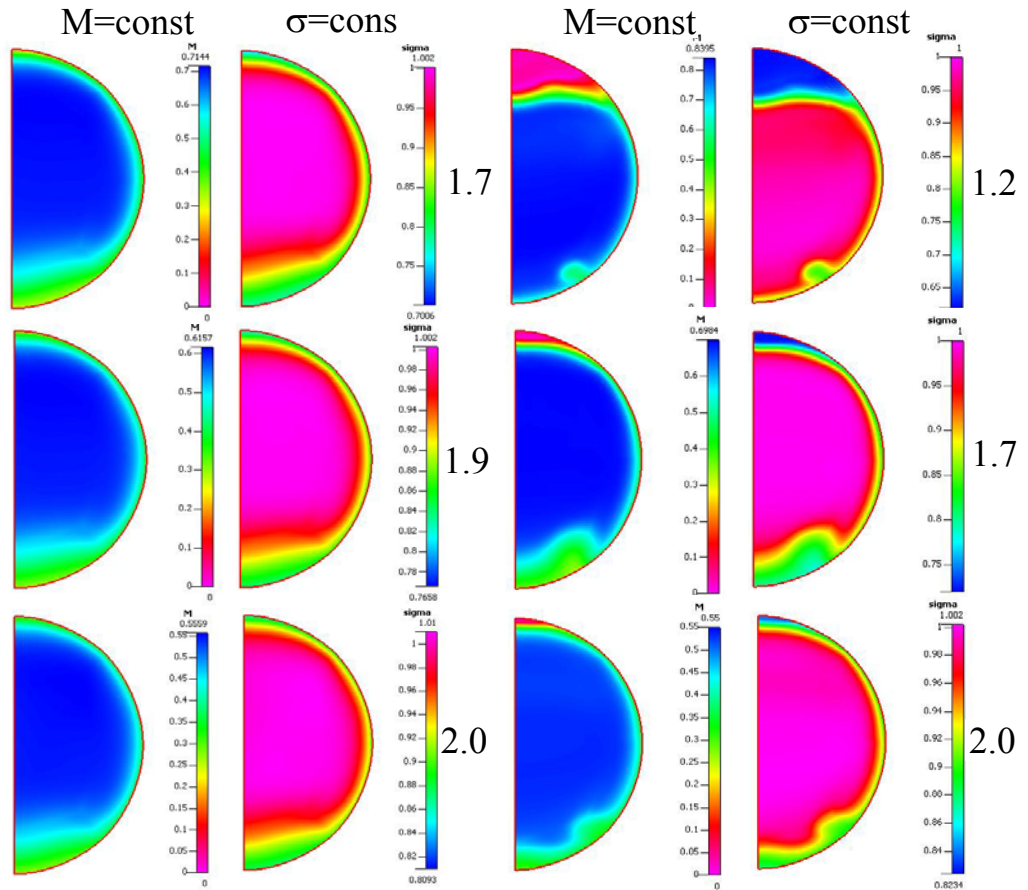


Fig. 11. Flow parameters - Mach number M and total pressure recovery coefficient σ at subsonic diffuser exit of 3D (left) and 2D (right) inlets under $M_\infty=1.2$ and throttling regime operation (figures in pictures correspond to $P_{thrott} / P_\infty = var$).

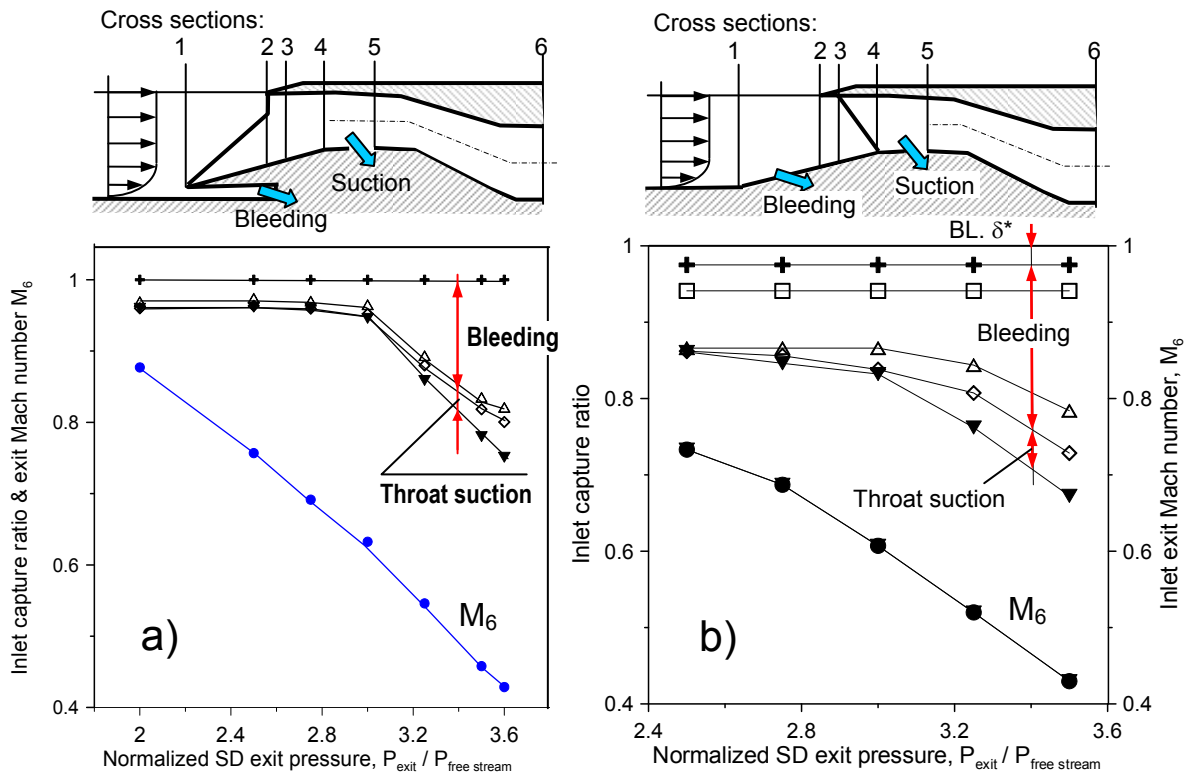


Fig. 12. Inlet capture ratio at different duct cross sections (Fig.3) and subsonic diffuser exit Mach number at $M_\infty=1.6$ vs throttling level P_{thrott} / P_∞ , a – 2D inlet, b – 3D inlet

\oplus - cross section “1”, \square - cross section “2”, \triangle - cross section “3”, \diamond - cross section “4”,
 \blacktriangledown - cross section “6”, \bullet - Mach number M_6

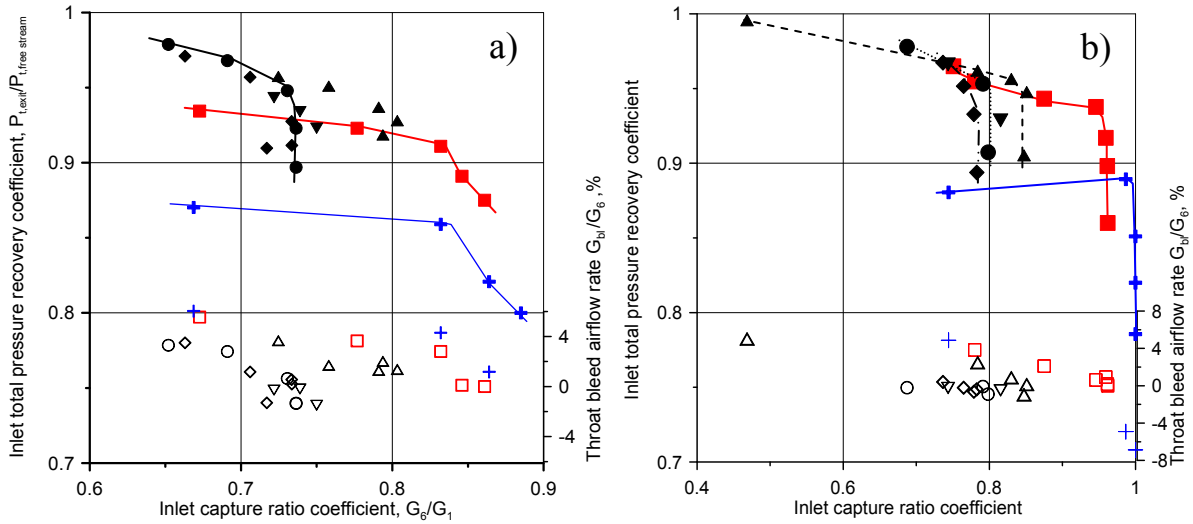


Fig. 13. Throttle performance and throat bleed airflow rate of 3-D – “a” and 2D – “b” inlets vs flight Mach number

M_∞	1.6	1.4	1.2	1.0	0.8	1.8
$P_{t, exit} / P_{t, \infty}$	■	▲	●	◆	▼	+
$G_{suct} / G_{inlet}, \%$	□	△	○	◇	▽	+

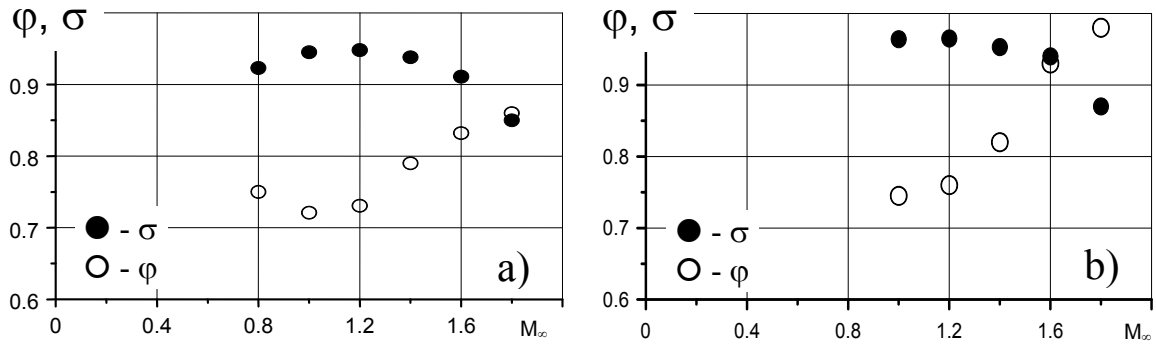


Fig. 14. Inlet performance σ and φ vs. flight Mach number under joint inlet/engine operation, a - 3D inlet, b - 2D inlet

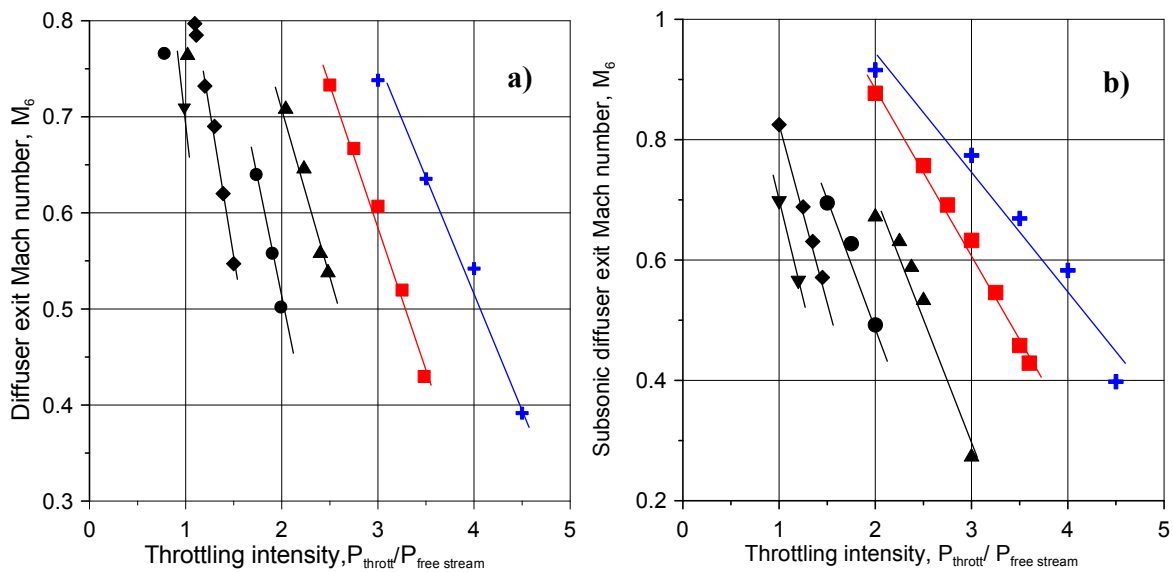


Fig. 15. Averaged Mach number at subsonic diffuser exit vs throttling intensity and flight M_∞ : a – 3D inlet, b – 2D inlet

M_∞	1.8	1.6	1.4	1.2	1.0	0.8
Sign	+	■	▲	●	◆	▼

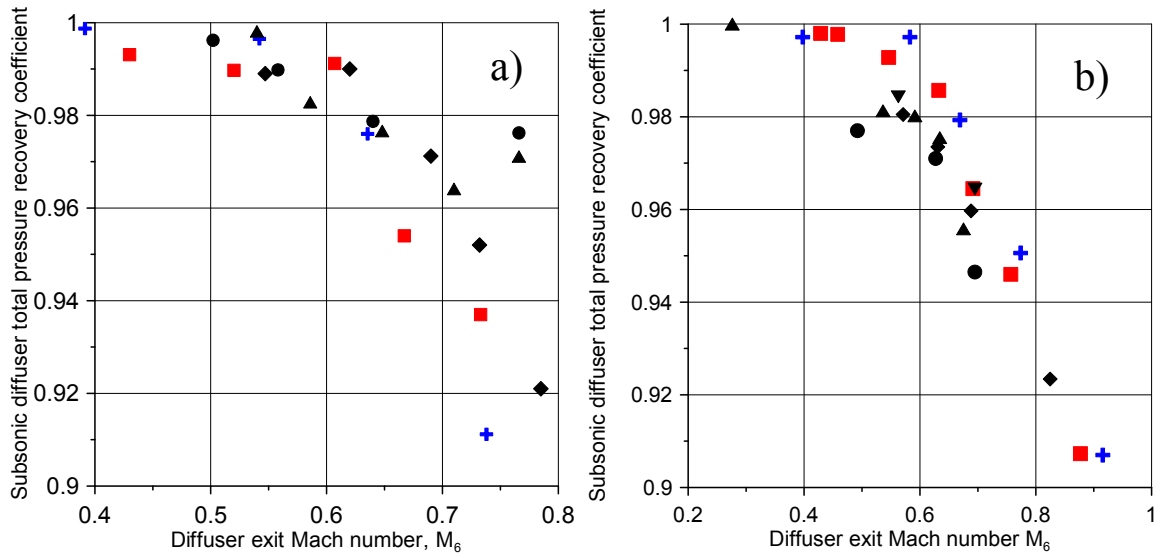


Fig. 16. Subsonic diffuser efficiency vs throttling mode: a – 3D inlet, b – 2D inlet

M_∞	1.8	1.6	1.4	1.2	1.0	0.8
σ_{SD}	+	■	▲	●	◆	▼

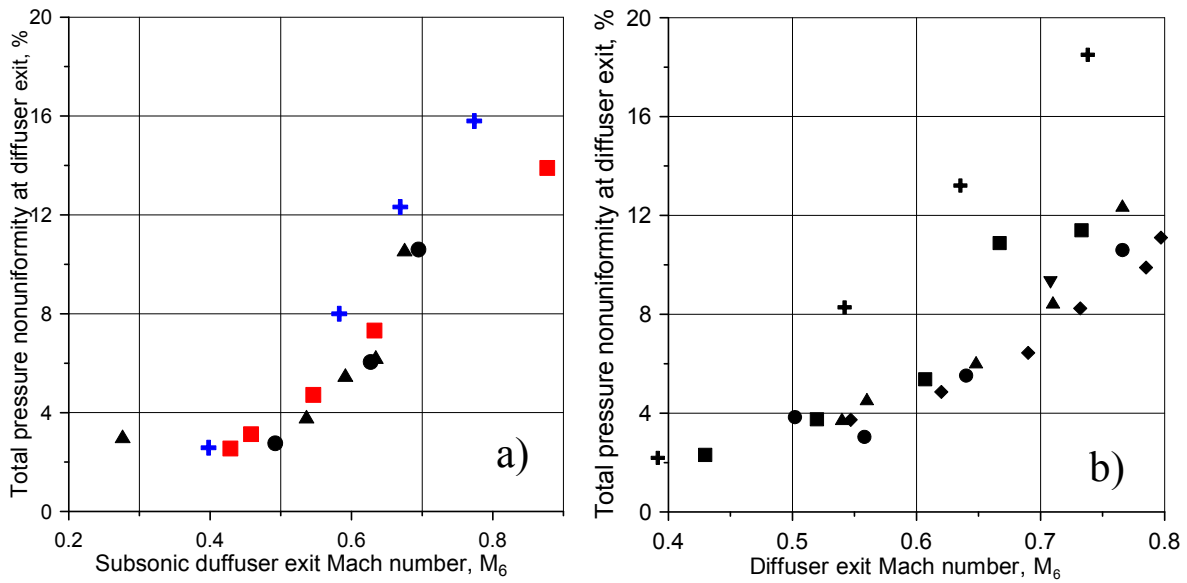


Fig. 17. Total pressure non uniformity parameter $\Delta\sigma$ vs Mach number at subsonic diffuser exit a – 2D inlet, b – 3D inlet

M_∞	1.8	1.6	1.4	1.2	1.0	0.8
$\Delta\sigma$	+	■	▲	●	◆	▼

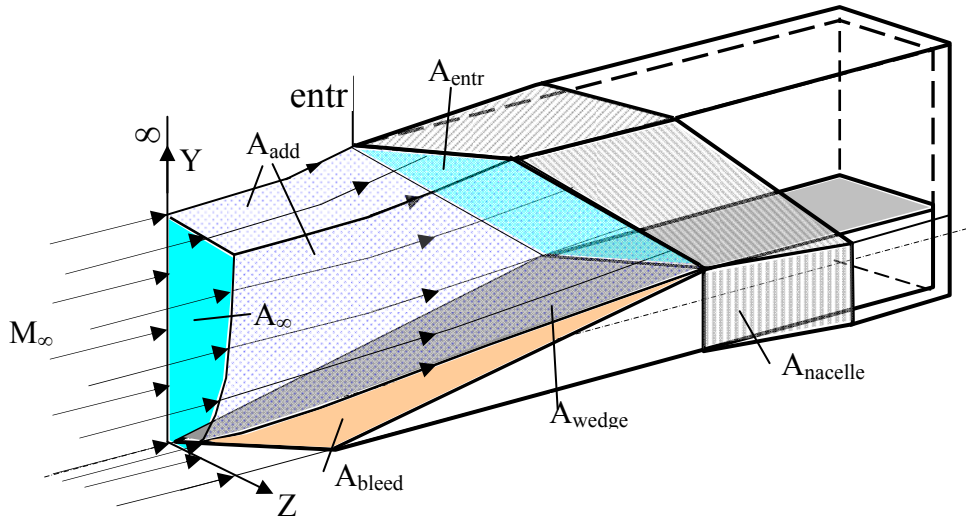


Fig. 18. Scheme of 3D inlet drag calculation

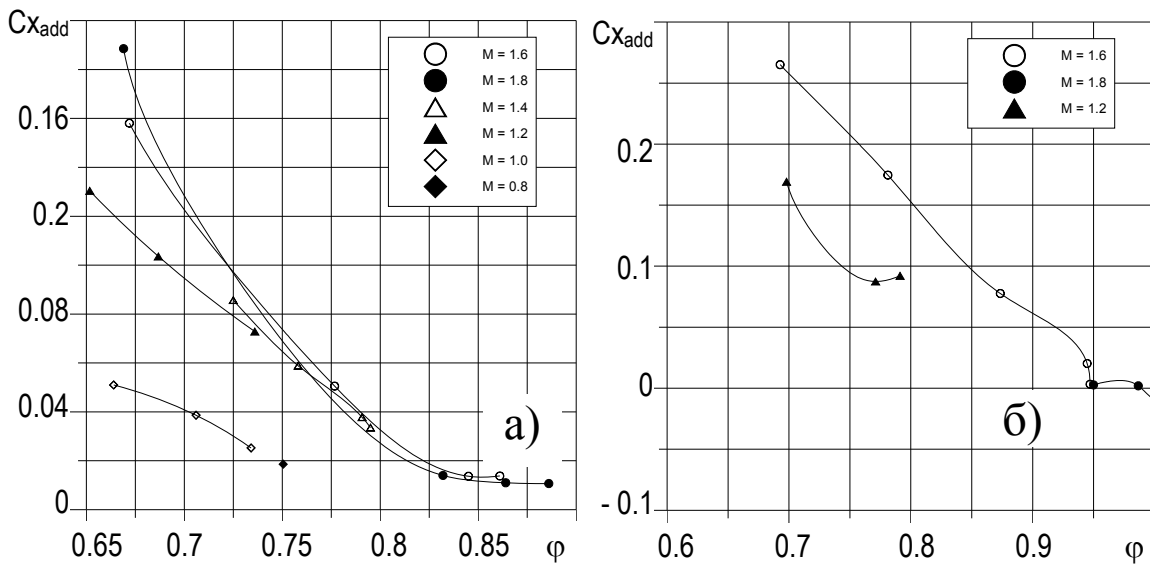


Fig. 19. Inlet additive drag coefficient vs inlet capture ratio at throttling regime operation
a – 3D inlet, b - 2D inlet

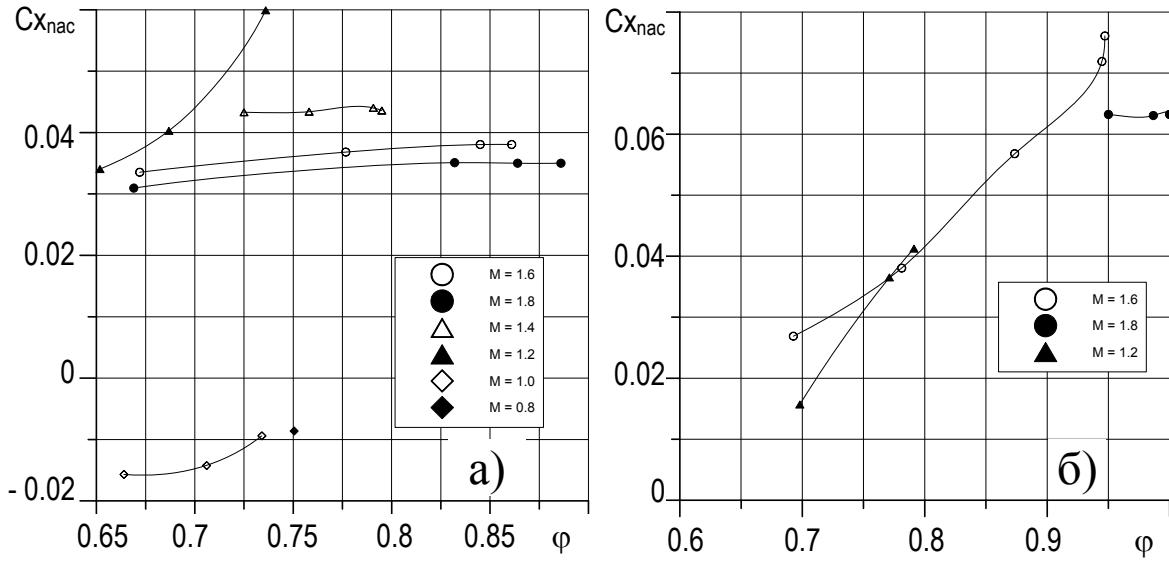


Fig. 20. Inlet nacelle drag coefficient $C_{x_{nac}}$ vs inlet capture ratio ϕ at throttling regime operation
a – 3D inlet, b - 2D inlet

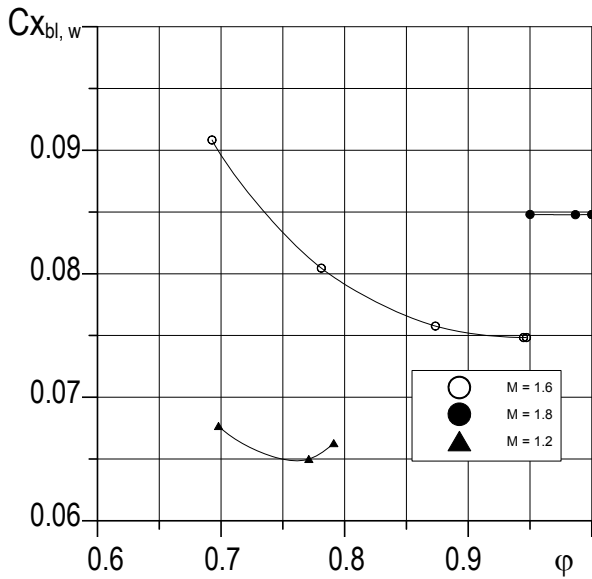


Fig. 21. Drag coefficient of 2D inlet bleeding wedge $C_{x_{bl,w}}$ at throttling regime operation

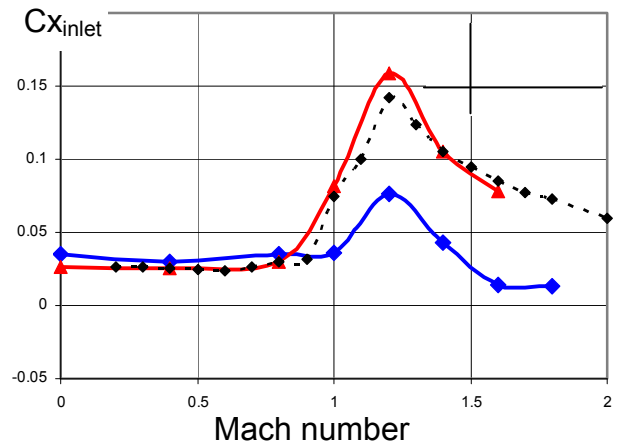


Fig.22 Total drag of inlets vs flight Mach number
—▲— - 2D inlet, —◆— - 3D inlet,
-●- - standard inlet